Physica E: Low-dimensional Systems and Nanostructures 111 (2019) 91–97

Contents lists available at ScienceDirect

Physica E: Low-dimensional Systems and Nanostructures

journal homepage: www.elsevier.com/locate/physe

Effect of the impurity on the Aharonov-Bohm oscillations and the intraband absorption in GaAs/$Ga_{1-x}Al_xAs$ quantum ring under intense THz laser field

M.G. Barseghyan[a,b], V.N. Mughnetsyan[a,c], L.M. Pérez[d], A.A. Kirakosyan[a], D. Laroze[d,*]

[a] Department of Solid State Physics, Yerevan State University, Alex Manoogian 1, 0025, Yerevan, Armenia
[b] National University of Architecture and Construction of Armenia, Teryan 105, 0009, Yerevan, Armenia
[c] Department of Physics, Yerevan State Medical University, Koryun 2, 0025, Yerevan, Armenia
[d] Instituto de Alta Investigación, CEDENNA, Universidad de Tarapacá, Casilla 7D, Arica, Chile

ARTICLE INFO

Keywords:
Aharonov-Bohm oscillations
Intense laser field
Quantum rings

ABSTRACT

The simultaneous effect of intense THz laser field and hydrogenic donor impurity on Aharonov-Bohm effect in a GaAs/$Ga_{1-x}Al_xAs$ single quantum ring is investigated using the non-perturbative Floquet theory in high-frequency limit and Ehlotzky approximation. It is shown that the intense THz laser field and donor impurity destroy the usual Aharonov-Bohm oscillations of the electron ground state. The Aharonov-Bohm-like oscillations of the excited energy levels, as well as the dipole, allowed optical transition energies can be effectively controlled by changing the laser field parameter and impurity position. Furthermore, an unusual oscillatory behavior is also observed for the dependence of optical transition intensity on magnetic field induction. The obtained results indicate the possibility of the prediction and effective control of electronic and optical properties of future devices on quantum rings.

1. Introduction

Since the first report on the self-assembly of semiconductor quantum rings (QR) [1], ring-shaped nanostructures have been attracting extensive attention as they offer a new platform to investigate the Aharonov-Bohm (AB) effect using spectroscopic techniques. The AB effect in QRs is a result of a quantum-interference phenomenon which may be detected by transport measurements [2]. Optical experiments have also identified the AB effect on a charged particle in a QR [3]. The effective controlling of AB oscillations is a powerful tool of tuning the electronic, magnetic and optical properties of QRs under the action of the magnetic field.

Theoretically, the effect of shape anisotropy on electronic, magnetic, and optical properties of QRs have been investigated by various authors [4–10]. The obtained results manifest that the magnitude of the AB oscillations strongly depends on the shape asymmetry. The role of electron-electron interactions on the AB effect was systematically explored via the exact diagonalization scheme for few interacting electrons in a QR [11–13]. Interactions were found to introduce fractional periodicity of the AB oscillations. Additionally, it has been shown that the AB oscillations can be controlled by varying of the electrons number. The influence of an in-plane electric field and eccentricity on the AB effect of a semiconductor QR has been investigated in Refs. [14,15]. It was pointed out that the electric field and the eccentricity destroy the rotational symmetry of the structure, and that is why these factors suppress the AB oscillations of the lower energy levels. Magneto-oscillations of the electric dipole moment has been predicted and analyzed in Refs. [16,17] for an electron confined in an infinitely narrow QR pierced by magnetic flux and subjected to an electric field in the ring plane. It has been shown that these oscillations are accompanied by periodic changes in the selection rules for inter-level optical transitions in the ring allowing control of polarization properties of the associated terahertz radiation. The emission spectrum of an AB QR placed into a single-mode quantum microcavity has been investigated in Ref. [18]. It was shown that the emission spectrum in the strong coupling regime has a multiplet structure and can be tuned by the variation of the magnetic field piercing the QR and by changing the strength and direction of the applied in-plane electric field.

On the other hand, the hydrogenic impurity problem in the semiconductor nanostructures is an essential task to grasp the electronic and optical properties of these structures. The presence of a hydrogenic impurity in QRs can be used as an additional way of controlling the electronic states and optical properties of QR [19,20]. The influence of hydrogenic impurities on AB oscillations in semiconductor QRs and its complexes has been investigated in Refs. [21–24]. The obtained results show that the presence of hydrogenic impurity can strongly affect, or

* Corresponding author.
E-mail address: dlarozen@uta.cl (D. Laroze).

https://doi.org/10.1016/j.physe.2019.03.003
Received 23 October 2018; Received in revised form 12 February 2019; Accepted 2 March 2019
Available online 08 March 2019
1386-9477/ © 2019 Elsevier B.V. All rights reserved.

even destroy, the AB oscillations.

Recently a few of our works were devoted to the study of the influence of intense THz laser field (ILF) on electronic and optical properties of single and double QRs [25–28]. Studies on the effect of electron-electron interaction and interdiffusion of heterojunction materials on AB oscillations and interband optical absorption in Gaussian-shaped double concentric QRs has also been reported [29,30]. The results show that the rendering of different shapes of just a single sample of a concentric double QR is realizable with an ILF, that in its turn, allows the manipulation of electronic and intraband optical properties of a structure. Very recently the anisotropy effect induced by the ILF on AB oscillations in isotropic and anisotropic single QR have been investigated in Ref. [31]. It was demonstrated that in isotropic QRs the ILF could create unusual AB oscillations that are characteristics of anisotropic QRs. Besides, in the case of anisotropic QRs, the ILF can be employed as an anisotropy controlling tool, since it is possible to visualize both the isotropic and the anisotropic properties of the ring.

The aim of this article is to analyze the theoretical investigation of the simultaneous effect of a THz ILF and hydrogenic donor impurity on AB effect and optical transitions in an isotropic QR. The manuscript is organized as follows: In Sec. 2 the theoretical model is presented. In Sec. 3 the numerical results are shown and analyzed. Finally, the conclusions are given in Sec. 4.

2. Theoretical framework

We consider a two-dimensional QR of cylindrical symmetry containing single electron and hydrogenic donor impurity positioned on one of the radial axes of the structure (chosen as the x-axis), under the action of the magnetic field which is directed perpendicular to the ring-plane. The system is radiated by ILF which is represented by a monochromatic plane wave of frequency ν [32]. The laser beam is non-resonant with the semiconductor structure [34] and linearly polarized along the x-axis. The time-dependent Schrödinger equation describes the electron motion [33]:

$$\frac{1}{2m}(\hat{\boldsymbol{\pi}}^2 + V(\mathbf{r}_\perp))\Phi(\mathbf{r}_\perp, t) = i\hbar\frac{\partial\Phi(\mathbf{r}_\perp, t)}{\partial t}, \tag{1}$$

where m is the electron effective mass, e is the electron charge, and $\hat{\boldsymbol{\pi}} = \hat{\mathbf{p}} - e(\mathbf{A}(t) + \mathbf{A}_m)/c$, such that $\hat{\mathbf{p}}$ is the two-dimensional momentum operator of the electron, $\mathbf{A}(t) = \mathbf{e}_x A_0 \cos(2\pi\nu t)$ is the laser field vector potential, where $\mathbf{e}_x$ denotes the unit vector on the x-axis, ν is the ILF frequence. Also, $\mathbf{A}_m$ denotes the vector potential of the magnetic field which is chosen to be $\mathbf{A}_m = (0, Bx, 0)$. In this case the scalar product $(\mathbf{A}(t)\cdot\mathbf{A}_m) = 0$. The potential, $V(\mathbf{r}_\perp) = V_{conf}(\mathbf{r}_\perp) + V_{coul}(\mathbf{r}_\perp)$, is the sum of confinement potential (V_{conf}) and the Coulomb potential (V_{coul}). For the confinement potential we choose the model of finite square-well:

$$V_{conf}(\mathbf{r}_\perp) = \begin{cases} 0, & \text{if } R_1 \le \sqrt{x^2 + y^2} \le R_2, \\ V_0, & \text{otherwise}, \end{cases} \tag{2}$$

where R_1 and R_2 are the inner and outer radii of the QR, respectively. Using the dipole approximation and Kramers-Henneberger unitary transformation [35,36] in the high-frequency regime the laser-dressed energies of the QR can be obtained from the following time-independent Schrödinger equation [27,28,31,32,37–40]:

$$\left(\frac{1}{2m}\left(\hat{\mathbf{p}} - \frac{e}{c}\mathbf{A}_m\right)^2 + V_d\right)\Phi_d = E_d\Phi_d\,, \tag{3}$$

where $V_d(\mathbf{r}_\perp) = V_{dconf}(\mathbf{r}_\perp) + V_{dcoul}(\mathbf{r}_\perp)$. In particular, $V_{dconf}(\mathbf{r}_\perp)$ is the time-averaged laser-dressed potential that can be expressed by the following expression [25,26,31]:

$$\begin{aligned} V_{dconf}(\mathbf{r}_\perp) = \frac{V_0}{\pi}Re\Big[&\pi - \theta(\alpha_0 - x - \Gamma_1)\arccos\left(\tfrac{\Gamma_1 + x}{\alpha_0}\right) \\ &+ \theta(\alpha_0 - x - \Gamma_2)\arccos\left(\tfrac{\Gamma_2 + x}{\alpha_0}\right) \\ &- \theta(\alpha_0 + x - \Gamma_1)\arccos\left(\tfrac{\Gamma_1 - x}{\alpha_0}\right) \\ &+ \theta(\alpha_0 + x - \Gamma_2)\arccos\left(\tfrac{\Gamma_2 - x}{\alpha_0}\right)\Big], \end{aligned} \tag{4}$$

where $\Gamma_i = Re(\sqrt{R_i^2 - y^2})$, $\theta(u)$ is the Heaviside unit-step function and $\alpha_0 = (e^2 I/2\pi^3 m^2 \varepsilon_h^{1/2} c\nu^4)^{1/2}$, which describes the strength of the laser field and comprises the intensity I, the frequency ν of the laser field, and the high-frequency dielectric constant ε_h. Note that I and ν can be chosen for a broad range in units of kW/cm^2 and THz, correspondingly [32]. In addition, the time-averaged laser-dressed impurity potential in the Ehlotzky approximation can be written as [41,42]:

$$V_{dcoul}(\mathbf{r}_\perp) = -\frac{e^2}{2\varepsilon}\left(\frac{1}{\sqrt{\Delta_+^2 + y^2}} + \frac{1}{\sqrt{\Delta_-^2 + y^2}}\right), \tag{5}$$

where ε is the dielectric constant of the material. For simplicity, ε is taken the same inside and outside the QR [43]. The static and high-frequency dielectric constants are related with the $\varepsilon = \varepsilon_h + (4\pi N e_T^2)(\omega_{TO}^2 M)^{-1}$, where M is the reduced mass of the solid, N is the number of unite cells per unite volume, e_T is the transverse dynamic effective charge and ω_{TO} is the long-wavelength transverse optical phonon frequency [44,45]. Here, $\Delta_\pm^2 = (x - x_0 \pm \alpha_0)^2$, such that x_0 is the impurity coordinate. More details of the derivation of Eq. (3) can be found in the Appendix A.

Note that when the impurity is not consider the system was recently studied in Ref. [31], and that when the magnetic field and impurity are not taken into account the reduced system was analyzed in Ref. [25]. Let us also remark that the eigenvalues of the laser-dressed energy E_d and the eigenfunctions $\Phi_d(x, y)$ can be obtained by solving Eq. (3) with the help of the exact diagonalization technique. The eigenfunctions are presented as a linear expansion of the one-electron wave functions in a rectangle with dimensions $L_x = L_y = L$:

$$\begin{aligned} \varphi_{n_x n_y}(x, y) = \frac{2}{L}sin\left(\frac{\pi n_x}{L}\left(x - \frac{L}{2}\right)\right)\times \\ \times\sin\left(\frac{\pi n_y}{L}\left(y - \frac{L}{2}\right)\right), \end{aligned} \tag{6}$$

where n_x and n_y are the quantum numbers. Here, L fixed at $L = 60$ nm. The rectangle is assumed to be concentric with the considered QR [25,26,31,46]. In our calculations, we have used 361 basis states which are appropriate for determining the energy eigenvalues of ground and few excited states. We have also considered the intra-band optical transitions in the conduction band. For x-polarization of the incident light the intensity of absorption in the dipole approximation is proportional to the square of the dipole matrix element $M_{fi} \sim \langle f|x|i\rangle$, when the transition goes from the initial state $|i\rangle$ to the final state $|f\rangle$. Moreover, the absorption coefficient is given as follows [47]:

$$\alpha(\omega) = \frac{A\Gamma|M_{fi}|^2}{(\hbar\omega - \Delta E)^2 + \Gamma^2}, \tag{7}$$

where $\Gamma = 0.4$ meV describes the broadening of the threshold energy [44], and A is a constant. In this manuscript, we always consider $|i\rangle$ to be the ground state. In the next section, we will discuss the numerical results for different sets of parameters.

3. Results and discussion

Our numerical calculations are carried out for GaAs/$Ga_{1-x}Al_xAs$ QRs with the following parameter values: $V_0 = 228$ meV (which corresponds to the value of $x \approx 0.3$). The effective mass in the whole heterostructure is taken $m = 0.067m_0$ (m_0 is the free electron mass) and

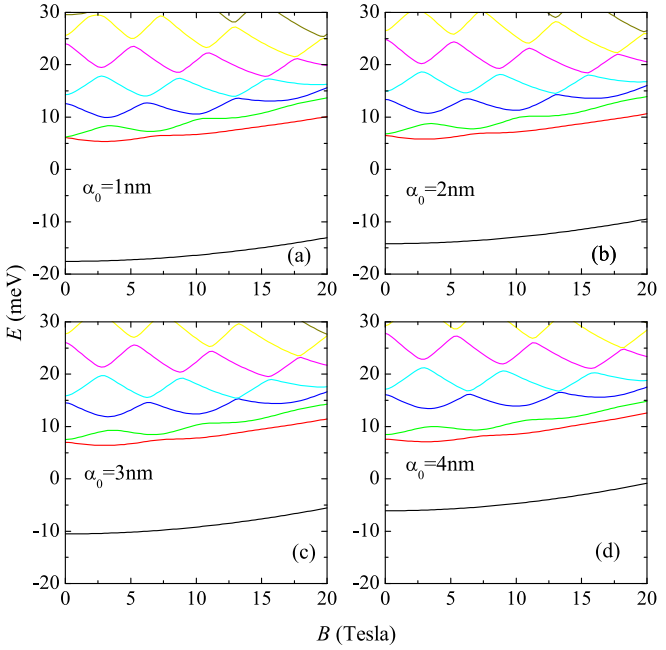


Fig. 1. The dependences of low-lying energy levels of electron on the magnetic field B for $x_0 = (R_1 + R_2)/2 = 12.5$ nm and for different values of ILF parameter α_0.

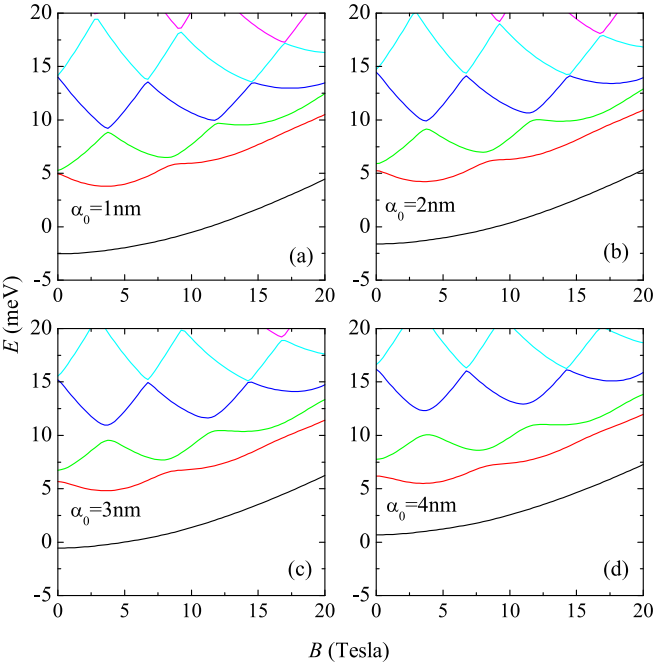


Fig. 2. The dependences of low-lying energy levels of electron on the magnetic field B for $x_0 = R_1 = 5$ nm and for different values of ILF parameter α_0.

$\varepsilon_h = 10.9$ [44,45,48]. Notice that the effective mass mismatch in the well and barrier regions will result only to a small quantitative change in our obtained result and the exact diagonalization technique is valid in this case also [49]. The inner and outer radii of QR are $R_1 = 5$ nm and $R_2 = 20$ nm. We consider three different positions of the donor impurity: 1) in the middle, 2) at the inner border and 3) at the outer border of QR.

In Fig. 1 the magnetic field dependencies of several low-lying energy levels for an impurity located in the middle of QR are presented for different values of the ILF parameter. Both the impurity and ILF break the cylindrical symmetry of the system, leading to violation of the Aharonov-Bohm oscillations. As a result, one can observe a ground state energy level isolated from others and revealing no oscillations. The higher levels show anti-crossings because the angular momentum is no longer a conserving quantity. On the other hand, note that with the increase of the laser field the effective length of the confining potential along the laser field polarization (x-direction) decreases in the lower part of the QR confinement potential [25]. Comparing the frames *a–d* of Fig. 1, one can observe that ILF mainly influences on the energy level of ground state and shifts it up, closer to the higher levels.

Fig. 2 demonstrates the dependencies of electron energy on magnetic field induction when the impurity is at the inner border of QR. The comparison with Fig. 1 shows that the ground state energy has higher values for an impurity, located on the edge of QR due to the weaker confining effect of the impurity potential on the electron (the maximum of the electron probability density is near the middle of the ring). The same can also be stated for the impurity located at the outer border of QR (see Fig. 3). One can also observe that the anti-crossings of the curves in Fig. 2*a* are negligible compared to ones in Fig. 1*a*. This fact shows that the role of "on-border" impurity in the breaking of the symmetry of higher states is tiny. Besides that, when the electron localization region is closer to the axis of the system, the electron is not sensitive concerning the potential symmetry breaking by ILF. However, for larger values of ILF parameter (Fig. 2 *b–d*) the effect of dressing is considerable even for $x_0 = R_1$ and the anti-crossings of the curves become more pronounced.

The highest energy levels are observed for the impurity center located at the outer border of QR, as it is shown in Fig. 3. From this figure,

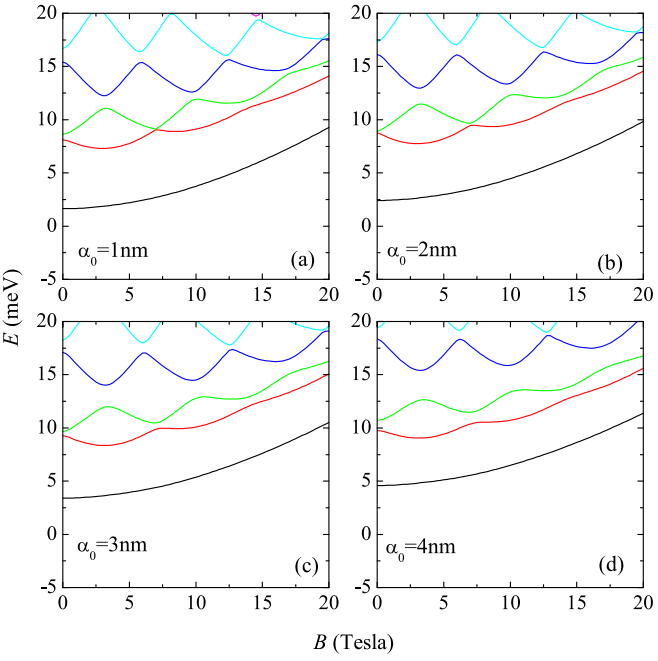


Fig. 3. The dependences of low-lying energy levels of electron on the magnetic field B for $x_0 = R_2 = 20$ nm and for different values of ILF parameter α_0.

we can notice that anti-crossings are pronounced for all considered values of the ILF parameter. From the comparison with the previous figures, one can observe a smaller magnitude of the energy oscillations due to the weaker effect of the magnetic field on the electron far from the region enclosed by the magnetic length. Note that here the magnetic length $l_B \approx 6$ nm. These results have good agreements with two limiting cases. In the absence of impurity the dependences of low-lying energy levels of the electron on the magnetic field for different values of ILF parameter are in good agreement with results obtained in Ref. [31]. In the absence of impurity and magnetic field for the fixed values of ILF parameter the energy values are in good agreement with the results

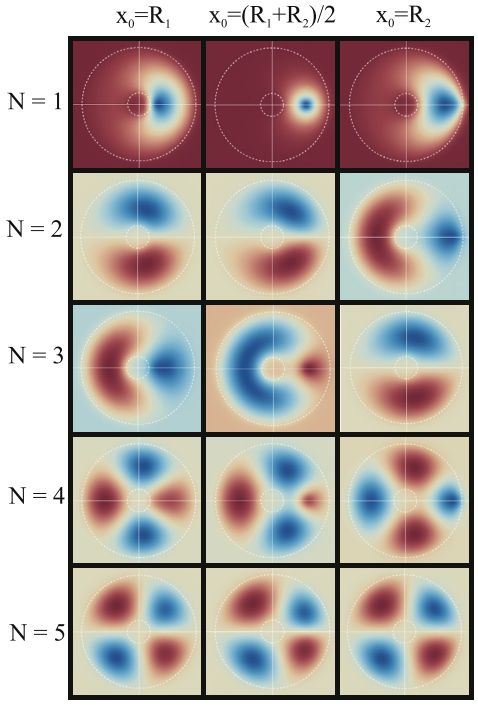


Fig. 4. The density plots of the wave functions of first five states for different values of impurity position x_0. The results are for $\alpha_0 = 1$ nm and $B = 0$.

published in the Refs. [25,26].

The density plots of the electron wave function is depicted in Fig. 4. The results are presented for different values of impurity position x_0 at $B = 0$ for a fixed value of α_0. We can observe that the electron cloud is no longer ring shaped as it must be in the absence of the impurity, but is centred at the impurity site. On the other hand, the physics behind the behaviors of the matrix elements of the optical transitions, which will be considered here, can be explained using the wave function distributions of corresponding states [50].

The intraband absorption for the optical transitions from the ground impurity state to the 2nd (black dots), 3rd (red dots), 4th (green dots) and the 5th (blue dots) electronic state is presented in Fig. 5 – 7. The vertical axis corresponds to the absorption threshold, while the horizontal one represents the value of the external magnetic field induction B. The sizes of the dots are proportional to the corresponding transition probabilities (square of the transition matrix element). The threshold energy oscillations are signatures of the Aharonov-Bohm oscillations of the initial and the final states. As it was expected from the discussion of Figs. 1–3, the larger value of the threshold energy corresponds to the smaller intensity of the ILF and the impurity location in the middle of QR (Fig. 5*a*). It can be seen from Fig. 5 that all the considered region of the magnetic field induction can be divided into two regions. The first one, corresponds to the first oscillation of the threshold energy with a very weak transition probability for $1 \rightarrow 2$ transitions (black dots), while in the second region a much intensity of transitions is observed due to the increase of the wave functions overlap in the radial direction. An opposite regularity can be observed for $1 \rightarrow 3$ transitions (red dots). Namely, a much intensity of transitions for small values of magnetic field induction weakens with increasing of B due to the partial recovering of the cylindrical symmetry of the 3rd state.

The intensities of $1 \rightarrow 4$ and $1 \rightarrow 5$ transitions are very small for all the values of magnetic field induction due to a weak overlap of the corresponding wave functions. When the impurity is located on one of the QR's borders and so has a weaker effect on the wave function symmetry the $1 \rightarrow 3$ transitions stand out in very strong intensity comparing with other transitions (Fig. 6 and Fig. 7). Interestingly, that for “on-border” impurity the intensity of $1 \rightarrow 2$ transitions has a quasi-oscillatory behavior, with the same period as one of the energy oscillations. This issue is brightly appreciated when $x_0 = R_2$ as it is shown in Fig. 7. This fact may be the result of the periodical change of the symmetrization effect of magnetic field on the 2nd state due to the periodical change in the wave function phase shift during the rotation of electron.

Finally, Fig. 8 represents the dependencies of intraband absorption coefficient on incident photon energy for $x_0 = R_2 = 20$ nm and for different values of magnetic field induction B and ILF parameter α_0. Note that the two considerable peaks of absorption spectrum are the result of transitions between different states for different values of the ILF parameter. We can see that for large values of B, and α_0 the righter peaks of the absorption spectrum vanish in accordance with the calculated values of transition probabilities, while the magnetic field and the ILF have opposite influences on the left peaks. These results are in agreement with the transition intensities discussed in Fig. 7.

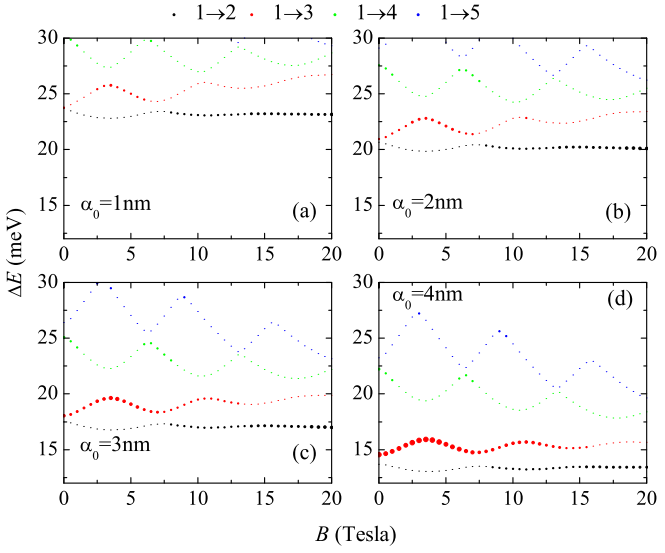


Fig. 5. The dependences of dipole allowed optical transition energies on magnetic field B for $x_0 = (R_1 + R_2)/2 = 12.5$ nm and for different values of ILF parameter α_0. The sizes of the dots are proportional to the intensities of the corresponding transitions.

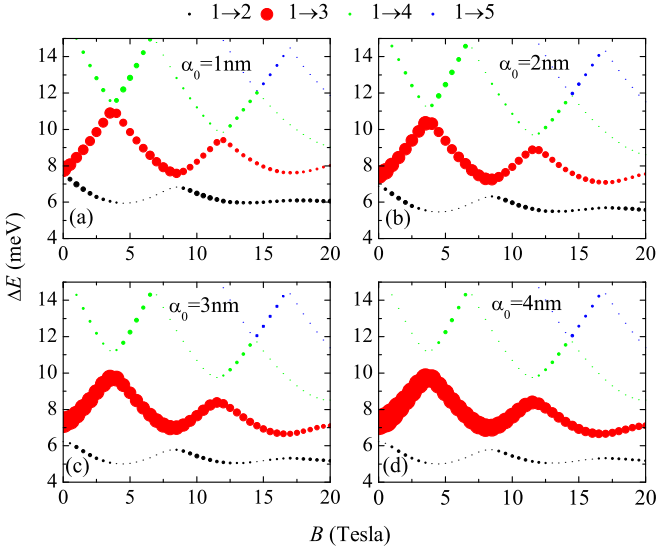


Fig. 6. The dependences of dipole allowed optical transition energies on magnetic field B for $x_0 = R_1 = 5$ nm and for different values of ILF parameter α_0. The sizes of the dots are proportional to the intensities of the corresponding transitions.

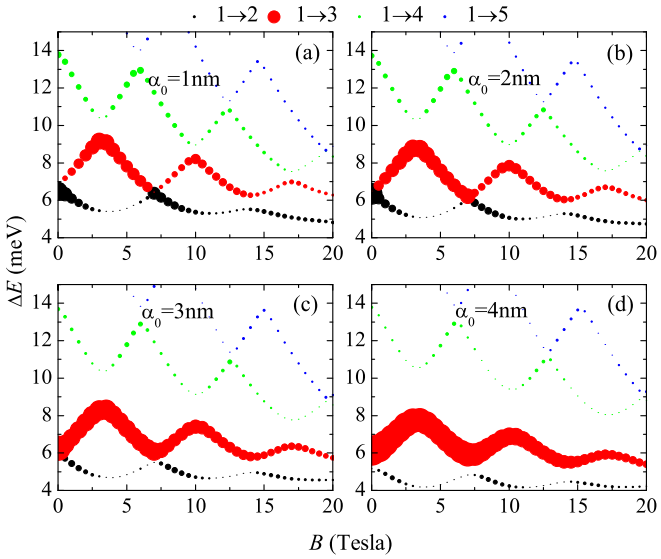


Fig. 7. The dependences of dipole allowed optical transition energies on magnetic field B for $x_0 = R_2 = 20$ nm and for different values of ILF parameter α_0. The sizes of the dots are proportional to the intensities of the corresponding transitions.

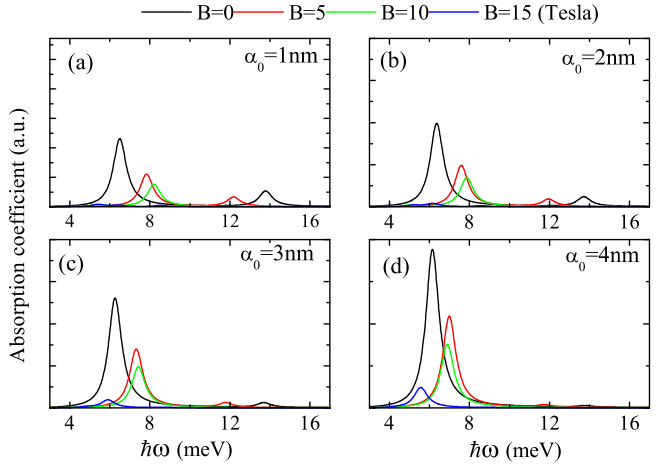


Fig. 8. The dependences of intraband absorption coefficient on incident photon energy for $x_0 = R_2 = 20$ nm and for different values of magnetic field induction and ILF parameter.

4. Final remarks

In conclusion, using the non-perturbative Floquet theory in high-frequency limit and Ehlotzky approximation, we have theoretically investigated the simultaneous effect of THz ILF and hydrogenic donor impurity on AB effect in anisotropic QR. The obtained results show that in the presence of hydrogenic impurity the electron ground state energy does not reveal any oscillations, while for the excited states the AB-like oscillations have been observed. The magnitude of these oscillations, as well as the dipole, allowed optical transition energies can be effectively controlled by changing the ILF parameter and impurity position. The strongest intensity of intraband optical absorption corresponds to the transitions of the electron from the ground state to the second excited state, when the impurity is on the outer border of QR. Additionally, an unusual oscillatory behavior is also observed for the dependence of optical transition intensity on magnetic field induction. We believe that the obtained results are useful and will open up new possibilities to the improved design and characterization of new devices based on single quantum rings, such as THz detectors, efficient solar cells, photon emitters, etc. Finally, it is worth to note that in this work we are interested only the monochromatic ILF because this particular case in the theory of laser-dressing of electron states is widely employed [37,38,40]. Extension on this direction will be presented in future works.

Acknowledgments

MGB and VNM acknowledge the financial support by the Armenian State Committee of Science (Project no. 18T-1C223). LMP and DL acknowledge partial financial support from FONDECYT 1180905. DL acknowledges partial financial support from Centers of excellence with BASAL/CONICYT financing, Grant FB0807, CEDENNA.

Appendix A

In this Appendix in more detail we present the derivation of Eq. (3) from Eq. (1). For this purpose let us remember that we have assumed that the laser field is under dipole approximation $\mathbf{A}(\mathbf{r}, t) \approx \mathbf{A}(t) = \mathbf{e}_x A_0 \cos(\omega_d t)$, where $A_0 = F_0 c/\omega_d$, F_0 is the electric field strength of ILF, $\omega_d = 2\pi\nu$. Besides, we have assumed that vector potential of the magnetic field is given by $\mathbf{A}_m = Bx\mathbf{e}_y$, which implies that $\mathbf{A}(t) \cdot \mathbf{A}_m = 0$. Under these two premises, one can perform the Kramers-Henneberger unitary translation transformation on the wave function $\Phi(\mathbf{r}_\perp, t)$ in order to transfer the time dependence from the kinetic to the potential term in the Hamiltonian operator at the left hand side of the Schrodinger equation (1). This transformation is explicitly given by Ref. [36]:

$$\Phi(\mathbf{r}_\perp, t) = \exp\left(\left(\frac{i}{h}\right)\boldsymbol{\alpha}\cdot\hat{\mathbf{p}}_\perp\right)\exp\left(\frac{i}{h}\frac{e^2}{2mc^2}\int A^2(t')dt'\right)\psi(\mathbf{r}_\perp, t), \tag{A.1}$$

where

$$\boldsymbol{\alpha}(t) = \frac{e}{m}\int \mathbf{A}(t')dt'.$$

Applying Eq. (A.1) into Eq. (1) one obtains the following time-dependent Schrödinger equation:

$$\left(\frac{1}{2m}\left(\hat{\mathbf{p}} - \frac{e}{c}\mathbf{A}_m\right)^2 + \tilde{V}\right)\psi(\mathbf{r}_\perp, t) = i\hbar\frac{\partial\psi(\mathbf{r}_\perp, t)}{\partial t}, \tag{A.2}$$

where $\tilde{V} = \tilde{V}(\mathbf{r}_\perp, t)$ is the laser dressed potential, which can be cast in the form

$$\tilde{V}(\mathbf{r}_\perp, t) = V(x + \alpha_0 \sin(\omega_d t), y). \tag{A.3}$$

Note that in (A.3) the term in x is the displacement of an electron due to its quiver motion in the laser field. We also point out that the Kramers-Henneberger transformation moves the time dependence from the laser potential to the scalar potentials. It is equivalent to change the laboratory frame of reference (related with the geometrical center of the QR structure) to the accelerated one, which follows the $\boldsymbol{\alpha}(t)$ quiver motion of the election. The potential $\tilde{V}(\mathbf{r}_\perp, t)$ is a periodic function on time (oscillating at frequency ω_d), which may be intuitively understood by changing the referential point of view from the semiconductor to the carrier's accelerate frame of reference.

Since Eq. (A.2) is a linear partial differential equation with periodic coefficients, it can be treated with the non-perturbative Floquet method [51]. This method was originally used for atoms under intense laser radiation [52]. Afterward, it has been extensively used for semiconductor low-dimensional structures. In general, in the framework of Floquet theory one tries to find the solution of Eq. (A.3) in terms of an infinite Fourier series of wave function $\psi(\mathbf{r}_\perp, t)$. Further, the potential term $\tilde{V}(\mathbf{r}_\perp, t)$ is also expanded in the Fourier series. As a consequence

$$\psi(\mathbf{r}_\perp, t) = \exp\left(-\frac{iEt}{\hbar}\right)\sum_{n=-\infty}^{\infty}\exp(-in\omega_d t)\phi_n(\mathbf{r}_\perp) \tag{A.4}$$

$$\tilde{V}(\mathbf{r}_\perp, t) = \sum_{n=-\infty}^{\infty}\exp(-in\omega_d t)U_n(\mathbf{r}_\perp, \alpha_0) \tag{A.5}$$

where

$$U_n(\mathbf{r}_\perp, \alpha_0) = \frac{1}{2\pi}\int_0^{2\pi} e^{in\omega_d t}V(x + \alpha_0 \sin(\omega_d t), y)dt$$

Inserting Eqs. (A.4) and (A.5) into Eq. (A.3), and after some straightforward calculations one can find that the Schrödinger equation is reduced to the infinite system of the time-independent coupled equations:

$$\left(\tfrac{1}{2m}\left(\hat{\mathbf{p}} - \tfrac{e}{c}\mathbf{A}_m\right)^2 + U_0(\mathbf{r}_\perp, \alpha_0)\right)\phi_n(\mathbf{r}_\perp) = (E + \hbar\omega_d n)\phi_n(\mathbf{r}_\perp) - \textstyle\sum_{m=-\infty}^{\infty} U_{n-m}(\mathbf{r}_\perp, \alpha_0)\phi_m(\mathbf{r}_\perp), \tag{A.6}$$

which is amenable to an iteration procedure. Details of this procedure can be found in Refs. [41,52].

Let us remark that, if the period $2\pi/\omega_d$ of the laser field is much longer than the characteristic transit time τ of the electron in the structure (that is the "adiabatic limit" $\omega_d\tau \ll 1$) the electron motion is dominated by the kinetic term of its unperturbed Hamiltonian and the electron is too fast "*to feel*" the effect of the field as a potential-well distortion. In the opposite case (that is "the high-frequency limit" $\omega_d\tau \gg 1$), the electron motion is dominated by the oscillation under the ILF and consequently the electron "*sees*" the averaged laser dressed potential. Here, we are interested only in the stationary states of an electron which appear once the high-frequency approximation of the Floquet method is applied. Namely, we assume that the frequency ω_d of laser field is considered to be very high so that the electron only "*feels*" the time-averaged of the laser-dressed confining potential. High values of (ω_d, A_0) can always be manipulated, meanwhile remaining in the range where dipole approximation and non-resonant laser field requirements are fulfilled Ref. [52]. For instance, it can be set up to MW/cm^2 for $GaAs/Ga_{0.7}Al_{0.3}As$ heterostructures. Therefore, in the high-frequency approximation only the zeroth-order solution of Eq. (A.6) contributes, which leads to

$$\left(\frac{1}{2m}\left(\hat{\mathbf{p}} - \frac{e}{c}\mathbf{A}_m\right)^2 + U_0\right)\phi_0(\mathbf{r}_\perp) = E\phi_0(\mathbf{r}_\perp), \tag{A.7}$$

where $U_0 = U_0(\mathbf{r}_\perp, \alpha_0)$. Let us particularize the scalar potential by $V(\mathbf{r}_\perp) = V_{conf}(\mathbf{r}_\perp) + V_{coul}(\mathbf{r}_\perp)$, where V_{conf} is confinement potential and V_{coul} is the Coulomb potential. In such case, we have that $U_0(\mathbf{r}_\perp, \alpha_0) = V_d(\mathbf{r}_\perp) = V_{dconf}(\mathbf{r}_\perp) + V_{dcoul}(\mathbf{r}_\perp)$, such that V_{dconf} is the laser-dressed confinement potential and V_{dcoul} is the laser-dressed Coulomb potential. Therefore, using the notation $\phi_0 = \Phi_d$ and $E = E_d$, we can rewrite Eq. (A.7) as follow:

$$\left(\frac{1}{2m}\left(\hat{\mathbf{p}} - \frac{e}{c}\mathbf{A}_m\right)^2 + V_d\right)\Phi_d = E_d\Phi_d, \tag{A.8}$$

which is the exactly time-independent Schrödinger equation (3).

References

[1] J.M. Garcia, G. Medeiros-Ribeiro, K. Schmidt, T. Ngo, J.L. Feng, A. Lorke, J. Kotthaus, P.M. Petroff, Appl. Phys. Lett. 71 (1997) 2014.
[2] A. Fuhrer, S. Lüscher, T. Ihn, T. Heinzel, K. Ensslin, W. Wegscheider, M. Bichler, Nature 413 (2001) 822.
[3] M. Bayer, M. Korkusinski, P. Hawrylak, T. Gutbrod, M. Michel, A. Forchel, Phys. Rev. Lett. 90 (2003) 186801.
[4] L. Wendler, V.M. Fomin, Phys. Rev. B 50 (1994) 4642.
[5] L. Wendler, V.M. Fomin, Phys. Status Solidi (b) 191 (1995) 409.
[6] J. Planeles, F. Rajadell, J.I. Climente, Nanotechnology 18 (2007) 375402.
[7] V.M. Fomin, V.N. Gladilin, S.N. Klimin, J.T. Devreese, N.A.J.M. Kleemans, P.M. Koenraad, Phys. Rev. B 76 (2007) 235320.
[8] A. Ghazaryan, A. Manaselyan, T. Chakraborty, Phys. Rev. B 93 (2016) 245108.
[9] G.O. de Sousa, D.R. da Costa, A. Chaves, G.A. Farais, F.M. Peeters, Phys. Rev. B 95 (2017) 205414.
[10] V.M. Fomin (Ed.), Physics of Quantum Rings, second ed., Springer International Publishing, Switzerland, 2018.
[11] T. Chakraborty, P. Pietiläinen, Phys. Rev. B 50 (1994) 8460.
[12] T. Chakraborty, P. Pietiläinen, Phys. Rev. B 52 (1995) 1932.
[13] T. Chakrabort, A. Manaselyan, M. Barseghyan, J. Phys. Condens. Matter 29 (2017) 075605.
[14] Z. Barticevic, G. Fuster, M. Pacheco, Phys. Rev. B 65 (2002) 193307.
[15] A. Bruno-Alfonso, A. Latgé, Phys. Rev. B 71 (2005) 125312.
[16] A.M. Alexeev, M.E. Portnoi, Phys. Rev. B 85 (2012) 245419.
[17] A.M. Alexeev, M.E. Portnoi, Phys. Status Solidi C 9 (2012) 1309.
[18] A.M. Alexeev, I.A. Shelykh, M.E. Portnoi, Phys. Rev. B 88 (2013) 085429.
[19] E.C. Niculescu, C. Stan, D. Bejan, C. Cartoaje, J. Appl. Phys. 122 (2017) 144301.
[20] D. Bejan, C. Stan, E.C. Niculescu, Opt. Mater. 75 (2018) 827.

[21] M. Aichinger, S.A. Chin, E. Krotscheck, E. Räsänen, Phys. Rev. B 73 (2006) 195310.
[22] P. Hui, Z. Jia-Lin, J. Phys. Condens. Matter 15 (2003) 7287.
[23] G.A. Farias, M.H. Degani, J.A.K. Freire, J. Costa e Silva, R. Ferreira, Phys. Rev. B 77 (2008) 085316.
[24] A.K. Manaselyan, M.G. Barseghyan, A.A. Kirakosyan, D. Laroze, C.A. Duque, Physica E 60 (2014) 95.
[25] A. Radu, A.A. Kirakosyan, D. Laroze, H.M. Baghramyan, M.G. Barseghyan, J. Appl. Phys. 116 (2014) 093101.
[26] A. Radu, A.A. Kirakosyan, D. Laroze, M.G. Barseghyan, Semicond. Sci. Technol. 30 (2015) 045006.
[27] H.M. Baghramyan, M.G. Barseghyan, D. Laroze, Sci. Rep. 7 (2017) 10485.
[28] H.M. Baghramyan, M.G. Barseghyan, A.A. Kirakosyan, J.H. Ojeda, J. Bragard, D. Laroze, Sci. Rep. 8 (2018) 6145.
[29] V.L. Aziz-Aghchegala, V.N. Mughnetsyan, A.A. Kirakosyan, Physica E 88 (2017) 157.
[30] V.L. Aziz-Aghchegala, V.N. Mughnetsyan, A.A. Kirakosyan, Physica E 96 (2018) 11.
[31] T. Chakraborty, A. Manaselyan, M. Barseghyan, D. Laroze, Phys. Rev. B 97 (2018) 041304(R).
[32] S. Ganichev, W. Prettl, Intense Terahertz Excitation of Semiconductors, Oxford University Press, 2006.
[33] B.G. Enders, F.M.S. Lima, O.A.C. Nunes, A.L.A. Fonseca, D.A. Agrello, F. Qu, E.F. Da Silva Jr., V.N. Freire, Phys. Rev. B 70 (2004) 035307.
[34] F. Qu, P.C. Morais, Phys. Lett. A 310 (2003) 460.
[35] H.A. Kramers, Collected Scientific Papers, North-Holland, 1956.
[36] W.C. Henneberger, Phys. Rev. Lett. 21 (1968) 838.
[37] M. Gavrila, J.Z. Kaminski, Phys. Rev. Lett. 52 (1984) 613.
[38] M. Pont, N.R. Walet, M. Gavrila, C.W. McCurdy, Phys. Rev. Lett. 61 (1988) 939.
[39] E.C. Valadares, Phys. Rev. B 41 (R) (1990) 1282.
[40] M. Gavrila, J. Phys. B At. Mol. Opt. Phys. 35 (2002) R147.
[41] (a) F. Ehlotzky, Phys. Lett. A 126 (1988) 524;
(b) Can. J. Phys. 63 (1985) 907.
[42] E.C. Niculescu, L.M. Burileanu, A. Radu, Superlattice. Microst. 44 (2008) 173.
[43] Z.Y. Deng, J.K. Guo, T.R. Lai, J. Phys. Condens. Matter 6 (1994) 5949.
[44] M. Sugawara (Ed.), Theoretical Bases of the Optical Properties of Semiconductor Quantum Nano-Structures, Semiconductors and Semimetals, vol. 60, Elsevier, New York, 1999.
[45] S. Adachi, Handbook on Physical Properties of Semiconductors vol. 2, Kluwer Academic Publishers, New York, 2004.
[46] S. Gangopadhyay, B.R. Nag, Nanotechnology 8 (1997) 14.
[47] K.A. Rodríguez-Magdaleno, R. Pérez-Álvarez, J.C. Martínez-Orozco, J. Alloy. Comp. 736 (2018) 211.
[48] S. Adachi, J. Appl. Phys. 58 (1985) R1.
[49] V.L. Aziz-Aghchegala, V.N. Mughnetsyan, A.A. Kirakosyan, Physica E 64 (2014) 41.
[50] R.C. Iotti, L.C. Andreani, Phys. Rev. B 56 (1997) 3922.
[51] P.A. Kuchment, Floquet Theory for Partial Differential Equations, Birkhauser, Basel, 1993.
[52] M. Gavrila, Atoms in Intense Laser Fields, Academic, New York, 1992.